Optical properties of epitaxial and polycrystalline $Sr_{1.8}Ca_{0.2}NaNb_5O_{15}$ thin-film waveguides grown by pulsed laser deposition

W. C. Liu, C. L. Mak,[a] K. H. Wong, D. Y. Wang, and H. L. W. Chan
Department of Applied Physics, The Hong Kong Polytechnic University, Hung Hom, Kowloon, Hong Kong SAR, China

(Received 3 January 2006; accepted 6 May 2006; published online 2 August 2006)

Epitaxial and polycrystalline ferroelectric $Sr_{1.8}Ca_{0.2}NaNb_5O_{15}$ thin films have been prepared by pulsed laser deposition on (100)MgO and fused quartz substrates, respectively. These films exhibit excellent surface flatness and high optical transmittance of about 80% over the whole visible region. Their good optical waveguide characteristics are demonstrated using prism coupling technique. Our results show that the internal scattering of the film is more influential in governing the propagation loss than the surface scattering, and that a heteroepitaxial growth of ferroelectric oxide films is essential for waveguide devices. © *2006 American Institute of Physics*. [DOI: 10.1063/1.2218471]

I. INTRODUCTION

Lead-based ferroelectrics such as $(Pb_{1-y}La_y)(Zr_{1-x}Ti_x)O_3$ (PLZT) and $(1-x)Pb(Mg_{1/3}Nb_{2/3})O_{3-x}PbTiO_3$ (PMN-PT) have long been studied for their applications in various electronic and electro-optic (EO) devices. Recent concerns of environmental hazard of using lead have led to renewed interest in lead-free materials. One of the well known lead-free ferroelectrics is the tetragonal-tungsten-bronze (TTB) structured $Sr_{1-x}Ba_xNb_2O_6$ (SBN). It has been studied for EO and nonlinear optical applications due to its large diagonal EO coefficient.[1–4] However, SBN has a low Curie temperature (20–180 °C, $0.25 \leqslant x \leqslant 0.75$) due to the existence of one void site in each unit cell. This makes it easily depolarized at ambient conditions. We can anticipate that if its Curie temperature can be further increased, SBN would be more useful for practical devices. Calcium-modified strontium sodium niobates $Sr_{2-x}Ca_xNaNb_5O_{15}$ (SCNN) ($x=0.05-0.35$), with 4*mm* symmetry and having a TTB structure similar to SBN, exhibits higher Curie temperatures (279–297 °C) due to the introduction of Na ions into the void sites.[5,6] Furthermore, SCNN exhibits extremely high transverse as well as longitudinal EO coefficients ($r_{51}=1100$ pm/V and $r_{33}=1320$ pm/V). SBN75 crystal, by contrast, has a longitudinal EO coefficient r_{33} of 1350 pm/V but a transverse EO coefficient r_{51} of only 42 pm/V.[7–9] Therefore optical waveguides based on SCNN films are highly desirable for efficient electro-optic applications such as low voltage phase and amplitude modulators, tunable lasers, and optical filters.

There are several reports on the dielectric, piezoelectric, and EO properties of SCNN crystals and ceramics.[5–7,10] The growth of large SCNN single crystals has been shown to be very difficult.[7] On the other hand, SCNN ceramics are easily fabricated. They, however, suffer from the typical disadvantages of being of a randomly oriented polycrystalline structure, optically opaque, and prone to various kinds of structural and chemical defects. The development of optical waveguide applications has fortuitously demanded the SCNN to be in thin-film form. Indeed, the fabrication of SCNN waveguides is very attractive because the optical confinement inherent in the waveguide structure allows a significant improvement in the efficiency of the EO and nonlinear optical applications. Optical waveguides can be achieved by depositing the SCNN films on a substrate of lower refractive index. Our previous work has demonstrated the epitaxial growth of SCNN films on MgO substrates.[8] In this paper, we reported the deposition of a SCNN layer on (100)MgO and fused quartz substrates to form air/SCNN/substrate waveguide structures. We focus on studying the relationship between microstructures and optical waveguide properties (i.e., refractive index, birefringence, transmittance, and propagation loss). Using a prism coupling technique, the TE and TM modes (*m* line) have been identified. From these observed modes, the thicknesses and refractive indices of the air/SCNN/MgO and air/SCNN/fused quartz planar waveguides are deduced. At the same time the excellent waveguide characteristics due to the large refractive index difference between SCNN ($n_{SCNN} \approx 2.28$ at 633 nm) and substrates ($n_{\text{fused quartz}}=1.46$ and $n_{MgO}=1.74$ at 633 nm) are clearly shown. The major light propagation loss mechanisms of these planar waveguides are also discussed.

II. EXPERIMENTAL CONDITIONS

SCNN targets were prepared by a conventional mixed-oxide process using analysis grade $SrCO_3$, $CaCO_3$, $NaHCO_3$, and Nb_2O_5 powders as the starting materials. These powders were weighted according to the molecular formula $Sr_{1.8}Ca_{0.2}NaNb_5O_{15}$ and subsequently ball milled for 12 h. After being calcined at 1200 °C for 6 h, the mixed powder was pressed into disk pellets and sintered at 850 °C for 2 h and then at 1250 °C for another 10 h. All as-prepared targets showed prominent SCNN crystalline phases by x-ray diffraction (XRD). The laser used for the pulsed laser deposition (PLD) process was a KrF excimer laser (Lambda Physik COMPex205, 248 nm, 20 ns), with a repetition rate of 10 Hz. The distance between the substrate and the target was fixed at 4 cm. The on-target laser energy density is about

[a]Author to whom correspondence should be addressed; FAX: 852-2333-7629; electronic mail: apaclmak@polyu.edu.hk

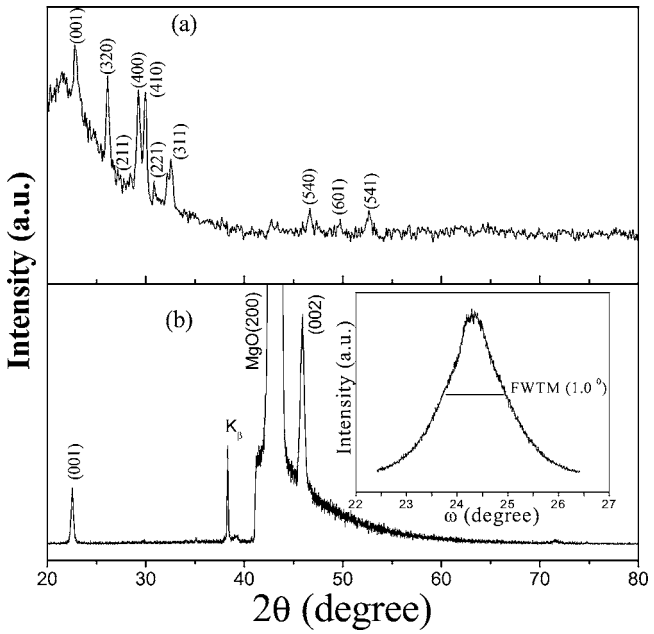

FIG. 1. X-ray diffraction patterns of SCNN films on (a) fused quartz and (b) MgO substrates. The inset is the rocking curve of the (200) SCNN peak of the SCNN/MgO film.

5 J cm^{-2}. (100)MgO and fused quartz substrates were placed side by side on the substrate holder. The SCNN films were deposited on both substrates simultaneously in the same experimental run at a substrate temperature of 740 °C and under an oxygen pressure of 150 mTorr. Immediately after the deposition, the films were *in situ* postannealed at growth temperature and 10 Torr oxygen ambient for 10 min before they were naturally cooled to room temperature to minimize oxygen deficiency.

The crystal structure of the deposited films was characterized by a four-circle x-ray diffractometer (Philips, X'pert) with Cu $K\alpha$ radiation operated at an acceleration voltage of 50 kV. Atomic force microscopy (AFM) (Nanoscope IV, Digital Instruments) was employed to examine the surface morphology of the films. The optical transmittance measurements were carried out by a two-beam spectrophotometer (Shimadzu UV-2101). The optical waveguide properties were examined by a prism coupling method (model 2010 prism, Metricon, USA) using a 632.8 nm laser beam.

III. RESULTS AND DISCUSSION

A. Structural properties and morphology

Figures 1(a) and 1(b) show the $\theta-2\theta$ patterns of the SCNN films on fused quartz and MgO substrates, respectively. Peaks with weak intensities, indicating poor crystalline quality, are observed in the SCNN/fused quartz films. This is mainly due to the amorphous structure of the fused quartz substrates. Nevertheless, (001), (320), and (311) SCNN peaks are still clearly and easily identified. The SCNN film on fused quartz is thus polycrystalline of pure TTB phase with cell lattice parameters of $c=3.899$ Å and $a=b=12.495$ Å. In the case of SCNN on MgO substrate, only strong reflections of (001) and (002) SCNN peaks are seen. No traces of other reflections are detected. The SCNN

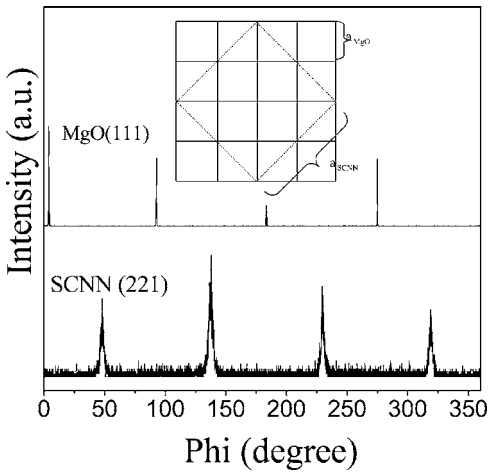

FIG. 2. Phi-scan pattern of SCNN films on MgO substrates. The inset is an illustration of one unit cell of SCNN corresponding to 16 unit cells of the MgO substrate.

film is of single phase and c axis oriented. The ω-scan rocking curve of the (002) SCNN peak, as shown in the inset of Fig. 1(b), displays a full width at half maximum (FWHM) of approximately 1.0°. To examine the texture of the in-plane films, φ scans of the following oblique planes were performed: (111) planes of MgO and (221) plane of SCNN. The results are shown in Fig. 2. Clear fourfold symmetry and 45° shift in their angular positions in the φ scans indicates a "diagonal-on-side" mode of SCNN on MgO. As shown in the inset of Fig. 2, two MgO diagonal units (4.22 Å $\times 2 \times \sqrt{2} \approx 12.45$ Å) match the side of one SCNN unit with a misfit of 4.2%. This therefore promotes an epitaxial growth of the SCNN film atop the MgO layer.

Figures 3(a) and 3(b) show the AFM images (3×3 μm^2) of SCNN films deposited on fused quartz and MgO, respectively. The surfaces are fairly homogeneous and free of any macroscopic extrusive features. The root-mean-square (rms) roughnesses of the SCNN/fused quartz film and SCNN/MgO film are 1.17 and 1.72 nm, respectively. The grain sizes of SCNN/fused quartz and SCNN/MgO films are about 80–100 and 60–80 nm, respectively. Our AFM images reveal that both SCNN thin films have smooth and dense surfaces, and the optical loss by surface scattering is expected to be low.

B. Optical transmission properties

Optical transmission measurements in the wavelength range of UV-visible-near-infrared have been carried out in

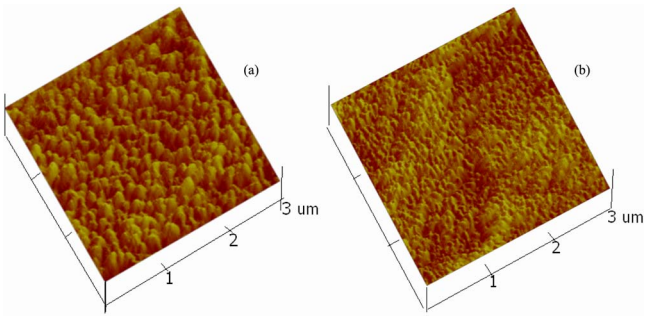

FIG. 3. (Color online) AFM images of SCNN films on (a) fused quartz and (b) MgO substrates.

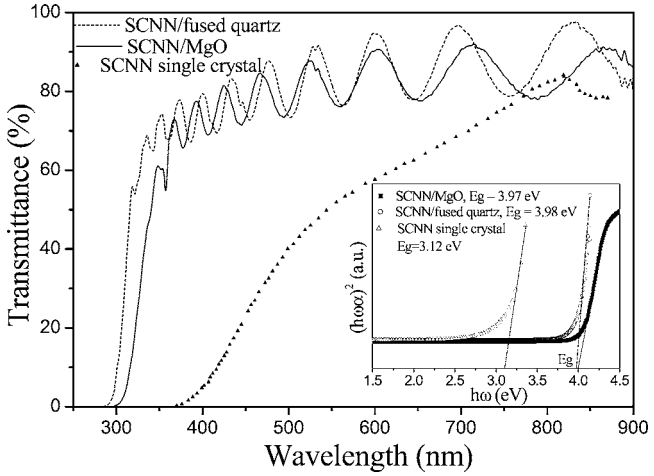

FIG. 4. The wavelength dependence of transmittance for SCNN films on fused quartz and MgO substrates. The inset is plots of $(h\omega\alpha)^2$ as a function of $h\omega$ for SCNN/fused quartz and SCNN/MgO films. The transmittance of SCNN single crystals is obtained from Ref. 8.

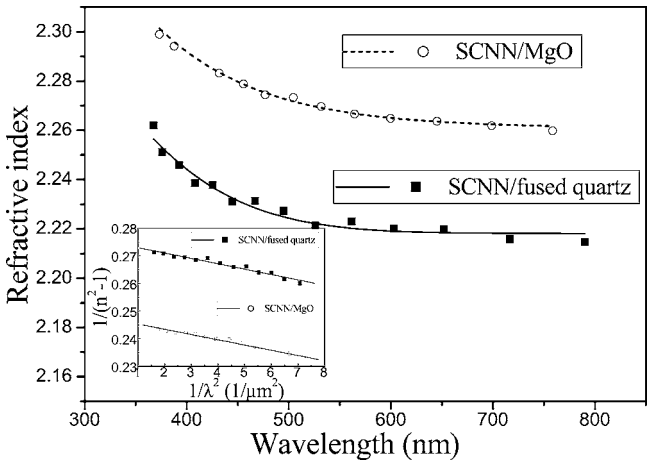

FIG. 5. Dispersion of the refractive index of SCNN films on fused quartz and MgO substrates obtained by optical transmission data. The inset is plots of $1/(n^2-1)$ as a function of $1/\lambda^2$.

order to determine the refractive index of the SCNN films. Optical transmission $T(\lambda)$ spectra (Fig. 4) for SCNN films deposited on transparent MgO and fused quartz substrates were measured using a double beam spectrophotometer. Both the SCNN/MgO and SCNN/fused quartz films exhibit about 80% transmittance from 400 to 900 nm. The well structured and smooth oscillations of the transmittance profiles indicate that the films have flat surfaces and uniform thicknesses. The transmittance of SCNN single crystals[8] is also plotted in the figure for comparison. The inset curves plot $(h\omega\alpha)^2$ as a function of $h\omega$ for SCNN/MgO and SCNN/fused quartz thin films. The absorption coefficient α of the SCNN films near the absorption edge was calculated directly from transmittance T against wavelength using the following formula:[12]

$$\alpha = \frac{1}{d}\ln\left(\frac{1}{T}\right) \quad \text{and} \quad (\alpha h\omega)^2 \propto (h\omega - E_g), \tag{1}$$

where d is the thickness of the SCNN film, E_g is the optical band-gap energy, and $h\omega$ is the energy of the incident photon. By using intercept method, optical band-gap energies of the SCNN single crystal and SCNN films grown on MgO and fused quartz are found to be 3.12, 3.97, and 3.98 eV, respectively. A large difference in the band-gap energies between the single crystal and our films is obtained.

Following Manifacier *et al.*,[13] the long wavelength transmittance was employed to calculate the linear refractive index n. The calculated values of the refractive index n are shown in Fig. 5. The inset of Fig. 5 shows that $1/(n^2-1)$ decreases linearly with $1/\lambda^2$. This indicates that the refractive index of the SCNN films follows the Sellmeier dispersion relationship [here the refractive index $n(\lambda)$ stands for the ordinary refractive index at wavelength of λ]:[14]

$$n(\lambda)^2 - 1 = s_0\lambda_0^2/[1 - (\lambda_0/\lambda)^2]. \tag{2}$$

From the figure, we notice that the refractive indices of the epitaxial SCNN/MgO films are larger than those of the polycrystalline SCNN/fused quartz films at the same wavelength. Miyazaki and Adachi suggest that both the epitaxial and polycrystalline films have a number of void networks. Densely packed crystallites with fewer void networks in epitaxial films usually results in relatively larger refractive index.[15]

C. Waveguide properties

The prism coupling technique is a well-developed method to evaluate dielectric and ferroelectric waveguide structures. Compared with other methods, this technique is simple because only angle measurements are involved. Furthermore, this method is accurate and nondestructive. The model 2010 prism coupling experimental setup used to observe the m lines and to measure the propagation loss is presented in Fig. 6(a). The principle of model 2010 prism coupling has been described elsewhere.[16] In this setup, a rutile prism was used to couple the He–Ne laser to the wave-

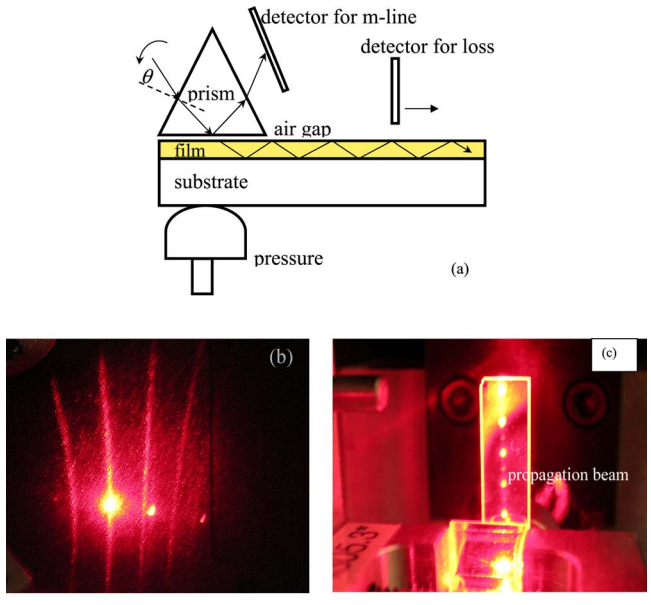

FIG. 6. (Color online) (a) Schematic drawing of the m lines and propagation loss measurement setup. (b) Photograph of the observed m lines of confined TE multimodes of the SCNN/MgO film. (c) Photograph of a screen image of the propagating 633 nm He–Ne laser beam in SCNN/MgO films.

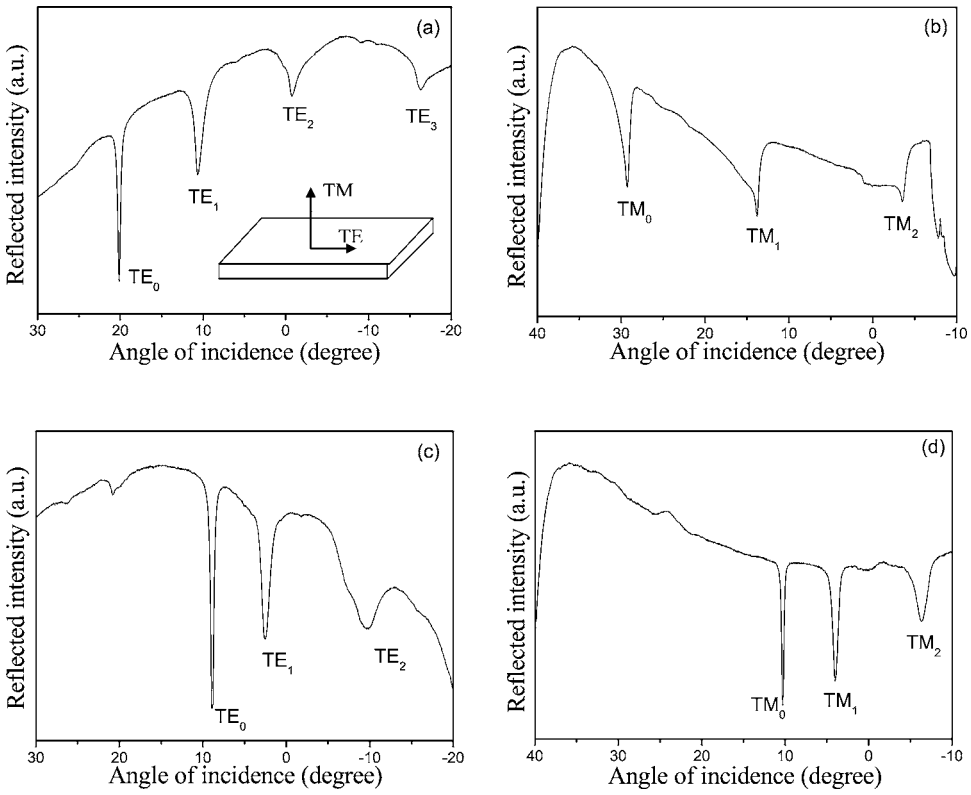

FIG. 7. Mode spectra of SCNN/MgO thin films in (a) TE and (b) TM polarizations and SCNN/fused quartz films in (c) TE and (d) TM polarizations.

guide structure. The angle of incidence θ of the laser beam was varied by using a rotary table upon which the prism, film, coupling head, and detector for *m* line were mounted. At certain discrete values of the incident angle, called mode angles, photons tunneled across the air gap into the waveguide and generated a guided optical propagation mode. This caused a sharp drop of light intensity reaching the detector. The laser beam was polarized with the electric field along the plane of the film (TE mode) or perpendicular to the film surface (TM mode). To measure the optical loss, θ was modulated to the mode angle in order to couple the laser beam into the waveguide film layer. The optical propagation loss was obtained by measuring the transmitted light intensity as a function of the propagation distances. As shown in Fig. 6(b), the observed *m* lines of confined TE modes of the SCNN films on MgO substrates are clear and sharp. The sharp and clear *m* lines imply that the SCNN thin films are of good optical waveguide quality. Similar *m* lines were also observed in the SCNN/fused quartz films. Figure 6(c) shows the photograph of a typical image of scattered light in the waveguide film layer. Laser beam was coupled into the waveguide at the prism side and detected by a mobile detector.

Figures 7(a)–7(d) show the TE and TM guided modes in the SCNN/MgO and SCNN/fused quartz films. Four TE-polarized and three TM-polarized guided modes are observed. SCNN is a uniaxial crystal of tetragonal structure with *c* axis as its optical polar axis. Our SCNN films are *c* axis oriented and epitaxially grown on (100)MgO substrates. Therefore, the measured n_{TE} and n_{TM} represent the ordinary refractive index n_o and the extraordinary refractive index n_e of the SCNN/MgO films, respectively. At a wavelength of 633 nm, our samples give $n_o=2.278$ and $n_e=2.183$. Our measured n_o is close to that of SCNN single crystals ($n_{\mathrm{SCNN\ crystal}}=2.280$).[6,11] The film thickness deduced from the guided mode data is 760 nm. It should be noted that there is a relatively large refractive index difference of 0.095 between n_{TE} and n_{TM}. Due to the tetragonal symmetry and epitaxial growth, the SCNN/MgO films have anisotropic optical properties. The anisotropy results in uniaxial birefringence, i.e., two different refractive indices for polarization parallel and perpendicular to the *c* axis.[17] For the SCNN/fused quartz films, n_{TE} and n_{TM} are determined to be 2.251 and 2.237, respectively. The randomly oriented polycrystalline tetragonal films results in a smaller birefringence, that is, a smaller difference between n_{TE} and n_{TM} (0.014), as compared to that of the anisotropic SCNN/MgO films. The thickness of the SCNN/fused quartz film is determined to be 990 nm.

In order to investigate the homogeneity and the interface properties of these SCNN films, we have reconstructed the refractive index profiles directly from the measured effective indices by using an improved version of the inverse Wentzel-Kramer-Brillouin (*i*WKB) method which only depends on the refractive index distributions within the guiding layer. More details of the said model are given by White and Heidrich.[18] Using a polynomial interpolation of the measured effective indices, we computed the refractive index profiles as a smooth function of the thickness. Figure 8 displays the evolution of the TE refractive index as a function of the layer thickness. For both the SCNN/MgO and SCNN/fused quartz films, the refractive index profiles indicate a step-index variation. Indeed, the refractive index remains constant within the guiding region and decreases rapidly near the film-substrate interface. Therefore, this step-index variation

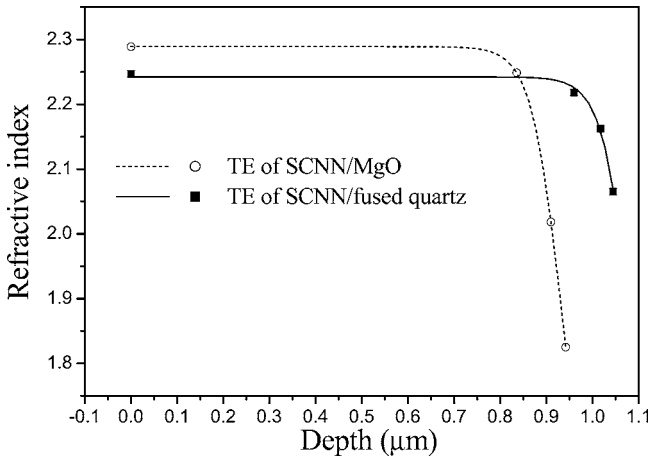

FIG. 8. TE refractive index profiles obtained by an inverse WKB method for SCNN films deposited on fused quartz and MgO.

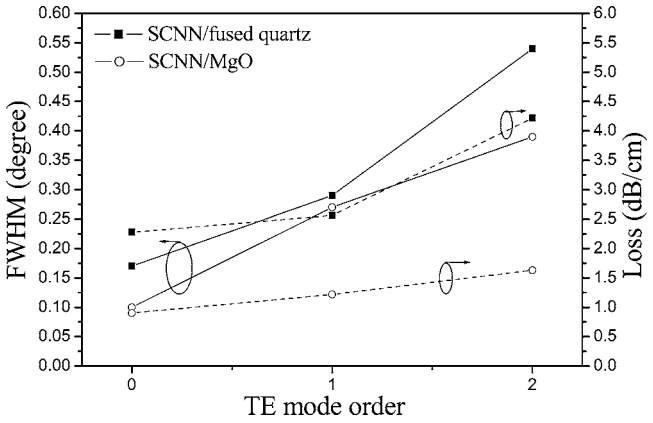

FIG. 10. Optical propagation loss and the FWHM of different order modes of TE guided modes coupled to the SCNN waveguide structures on MgO and fused quartz substrates.

is rather synonymous with a good optical homogeneity along the film thickness. The refractive index turning points of the SCNN/MgO and SCNN/fused quartz films are observed to be 760 and 950 nm, respectively. These are consistent with the film thickness deduced previously.

By varying the incident angle, all guided modes for the films could be separately excited, and the out-of-plane scattered light was visible as a streak that extend along the guide away from the prism, as shown in Fig. 6(c). The measured scattered intensities from the air/SCNN/MgO and air/SCNN/fused quartz planar waveguides are observed as a function of propagation along the guide, as displayed in Fig. 9. TE_0, TE_1, and TE_2 modes were excited in the SCNN films on MgO. A least-squares fit gives an optical loss α of 0.90 dB/cm for the TE_0 mode. Higher losses with 1.22 dB/cm for the TE_1 mode and 1.63 dB/cm for the TE_2 mode are also determined. The influence of the different substrates and crystalline quality on the propagation losses was found to be important, as observed in Fig. 9(b). We obtained losses of 2.28, 2.56, and 4.22 dB/cm for the TE_0, TE_1, and TE_2 modes of SCNN films on fused quartz, respectively. This shows that losses of the SCNN/fused quartz waveguide modes are larger than those of corresponding modes of the SCNN/MgO waveguide.

There are several sources of loss, such as absorption, leakage, internal scattering, surface scattering, and interface scattering.[19] Among these sources, internal scattering, interface scattering, and surface scattering seem to have major influences. The surface scattering loss depends mainly on the surface roughness. From our AFM results, the SCNN/fused quartz films have smoother surface with rms of 1.17 nm, as compared to that of the SCNN/MgO films with rms of 1.72 nm. This means that the SCNN/fused quartz films probably have smaller surface scattering loss than the SCNN/MgO films. But, in fact, our results show that the SCNN/MgO films have a much smaller optical loss compared to the SCNN/fused quartz films. This indicates that the internal scattering and the interface scattering, rather than the surface scattering, are dominant in our SCNN waveguide structures. Grain boundaries in optically isotropic media may induce refractive index discontinuities among grains. Refractive index discontinuities at grain boundaries will therefore effectively scatter light along the direction of propagation. Furthermore, any polycrystalline medium that is optically isotropic will scatter light if the crystalline orientation varies among grains. Hence, highly oriented thin films with good crystal quality could probably lower internal scattering.

Figure 10 shows the optical propagation loss and the FWHM of the TE guided modes coupled to the SCNN waveguide structures on MgO and fused quartz substrates as functions of the TE mode orders. For both SCNN/MgO and SCNN/fused quartz samples, the FWHM and the optical loss increase with mode order. There is a direct proportional relationship between the FWHM and the propagation loss. We

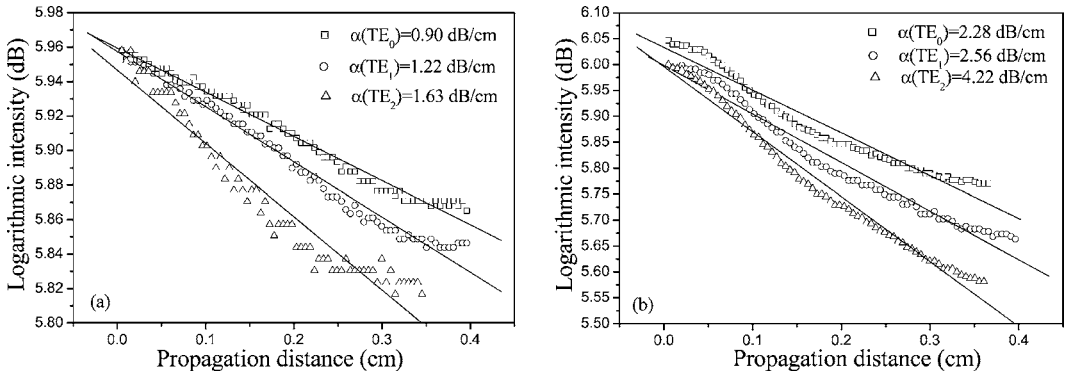

FIG. 9. Optical attenuation of the different order modes of the (a) SCNN waveguide on MgO and (b) SCNN waveguide on fused quartz.

notice that the FWHM and optical propagation loss of the TE_0 mode of the SCNN/MgO structure is reduced by around one-half and one-third in comparison to those of the SCNN/fused quartz waveguide, respectively. Finally, with increasing mode order, both the FWHM and propagation loss of the guided modes in the SCNN/MgO waveguide are smaller, indicating that SCNN/MgO waveguides have better performance than the SCNN/fused quartz waveguides.

IV. CONCLUSION

High transparent epitaxial SCNN films on (100)MgO and polycrystalline SCNN films on fused quartz have been successfully deposited by pulsed laser deposition. The surface morphologies of the thin films were observed to be very smooth with rms roughness of 1.17 nm for the SCNN/fused quartz films and 1.72 nm for the SCNN/MgO films. Refractive index dispersive curves following the Sellmeier equation were obtained from the measured transmittance curve using the Manifacier model. The polycrystalline SCNN/fused quartz film shows slightly low refractive indices compared to the epitaxial SCNN/MgO films. We have investigated the optical properties of the planar waveguides using the prism coupling technique. The ordinary (n_o) and the extraordinary (n_e) refractive indices of the SCNN/MgO films are determined to be 2.278 and 2.183, respectively. The relatively large index difference of 0.095 due to uniaxial birefringence is the result of anisotropic crystal microstructure. A small difference between n_o and n_e was found in the polycrystalline isotropic SCNN/fused quartz films. An optical propagation loss of 0.90 dB/cm for the TE_0 mode of the SCNN/MgO waveguide was measured. This is smaller than the 2.28 dB/cm of the SCNN/fused quartz waveguide. This result confirms the interest of using well oriented, textured, and crystallized thin films for integrated optics applications. A direct proportional relationship between the FWHM of the mode angle profile and the optical loss was observed.

ACKNOWLEDGMENTS

Part of this work was supported by a RGC research grant (PolyU 5291-02P) of HKSAR. One of the authors (W.C.L.) was supported by a Ph.D. studentship of the Hong Kong Polytechnic University. The authors would like to thank Dr. Xiong Qing of Wuhan University for his help and discussion in calculating the refractive index profile.

[1] P. Tayebati, D. Trivedi, and M. Tabat, Appl. Phys. Lett. **69**, 1023 (1996).
[2] Y. Y. Zhu, J. S. Fu, R. F. Xiao, and G. K. L. Wong, Appl. Phys. Lett. **70**, 1793 (1997).
[3] H. F. Cheng, G. S. Chiou, K. S. Liu, and I. N. Lin, Appl. Surf. Sci. **113/114**, 217 (1997).
[4] C. L. Mak, C. H. Luk, and K. H. Wong, Thin Solid Films **325**, 79 (1998).
[5] B. Yang, F. Li, J. P. Han, X. J. Yi, H. L. W. Chan, H. C. Chen, and W. Cao, J. Phys. D **37**, 921 (2004).
[6] R.-J. Xie, Y. Akimune, K. Matsuo, and T. Sugiyama, Appl. Phys. Lett. **80**, 835 (2002).
[7] R. R. Neurgaonkar, W. K. Cory, J. R. Oliver, E. J. Sharp, G. L. Wood, M. J. Miller, W. W. Clark, and G. J. Salamo, Mater. Res. Bull. **23**, 1459 (1988).
[8] Y. L. Zhang, C. L. Mak, K. H. Wong, and C. L. Choy, Thin Solid Films **449**, 63 (2004).
[9] Y. H. Xu, *Ferroelectric Materials and Their Application* (North-Holland, Amsterdam, The Netherlands, 1991), p. 83.
[10] R.-J. Xie and Y. Akimune, J. Mater. Chem. **12**, 3156 (2002).
[11] G. L. Wood and R. R. Neurgaonkar, J. Opt. Soc. Am. B **11**, 1211 (1994).
[12] W. Liu, A. Li, J. Tan, D. Wu, and N. Ming, Appl. Phys. A: Mater. Sci. Process. **81**, 543 (2005).
[13] J. C. Manifacier, J. Gasiot, and J. P. Fillard, J. Phys. E **9**, 1002 (1976).
[14] M. DiDomenico, Jr. and S. H. Wemple, J. Appl. Phys. **60**, 736 (1986).
[15] T. Miyazaki and S. Adachi, Jpn. J. Appl. Phys., Part 1 **31**, 979 (1992).
[16] W. Liu, D. Wu, A. Li, H. Ling, Y.-f. Tang, and N. Ming, Appl. Surf. Sci. **191**, 181 (2002).
[17] M. J. Bergmann, Ü. Özgür, H. C. Casey, Jr., H. O. Everitt, and J. F. Muth, Appl. Phys. Lett. **75**, 67 (1999).
[18] J. M. White and P. F. Heidrich, Appl. Opt. **15**, 151 (1976).
[19] J. S. Mir and J. A. Agostinelli, J. Vac. Sci. Technol. A **12**, 1439 (1994).